The Astrophysical Journal Letters, 893:L28 (4pp), 2020 April 20 https://doi.org/10.3847/2041-8213/ab8642

Optical Counterpart to the Ultraluminous X-Ray Source in the UGC 6456 Galaxy

A. Vinokurov[1], K. Atapin[2], and Y. Solovyeva[1]
[1] Special Astrophysical Observatory, Nizhnij Arkhyz, 369167, Russia; vinokurov@sao.ru
[2] Sternberg Astronomical Institute, Lomonosov Moscow State University, Universitetskij Pr. 13, Moscow 119992, Russia
Received 2020 January 27; revised 2020 March 30; accepted 2020 April 3; published 2020 April 17

Abstract

We report the identification of the optical counterpart to the transient ultraluminous X-ray source in the blue dwarf galaxy UGC 6456 (VII Zw 403). The source is highly variable in both the X-ray (by a factor of at least 100, 0.3–10 keV) and optical (by a factor of three, *V*-band) ranges. The peak X-ray luminosity of UGC 6456 ultraluminous X-ray source (ULX) exceeds 10^{40} erg s^{-1}; the absolute magnitude when the source is optically bright is $M_V = -8.24 \pm 0.11$, which makes this source one of the brightest ULXs in the optical range. We found a correlation between the optical and X-ray fluxes (with a coefficient of 0.9 ± 0.3), which may indicate that the optical emission is produced by re-processing of the X-rays in outer parts of the optically thick wind coming from the supercritical accretion disk. Optical spectra of UGC 6456 ULX show broad and variable hydrogen and helium emission lines, which also confirms the presence of the strong wind.

Unified Astronomy Thesaurus concepts: Accretion (14); X-ray binary stars (1811); X-ray point sources (1270); X-ray identification (1817)

1. Introduction

Ultraluminous X-ray sources (ULXs) are variable objects whose luminosity exceeds the Eddington limit for stellar mass black holes ($\geqslant 10^{39}$ erg s^{-1}), assuming isotropic emission. These objects are located outside the centers of galaxies; that is, they are not super-massive black holes. Early papers on ULXs suggested intermediate-mass black holes (IMBHs; 10^2–$10^4\,M_\odot$) as accretors in these systems (e.g., Colbert & Mushotzky 1999). However, studies of the last decade (Gladstone et al. 2009; Sutton et al. 2013; Fabrika et al. 2015; Pinto et al. 2016; Walton et al. 2018) have shown that observational properties of most ULXs can be explained by supercritical gas accretion onto black holes of stellar masses (from a few to several tens masses of the Sun), or even onto neutron stars. The last possibility has been convincingly confirmed by detection of coherent X-ray pulsations in six ULXs (Bachetti et al. 2014; Fürst et al. 2016; Israel et al. 2017; Carpano et al. 2018; Rodríguez Castillo et al. 2019; Sathyaprakash et al. 2019).

In contrast to the X-ray range, in the optical one ULXs are studied much more poorly. Only $\gtrsim$20 ULXs have been unequivocally identified using the Hubble Space Telescope (HST) data. All of them are faint sources with visual magnitudes of $m_V = 21$–26 (Tao et al. 2011; Gladstone et al. 2013). Moreover, most ULXs are associated with star-forming regions (e.g., Poutanen et al. 2013) and located in crowded regions, which makes it difficult to study them with ground-based telescopes.

Here we present the identification of the optical counterpart to the ULX in the galaxy UGC 6456 (VII Zw 403), which is one of the closest blue compact dwarf galaxies ($D = 4.54$ Mpc, Tully et al. 2013). UGC 6456 ULX is a transient ULX: its X-ray luminosity changes by more than two orders of magnitude with a peak value of 1.7×10^{40} erg s^{-1} in the 0.3–8 keV energy range (Brorby et al. 2015). In the bright state, the sources shows a very hard power-law spectrum with a photon index of $\Gamma \sim 1$. We report the presence of a correlation between the long-term X-ray and optical variability of UGC 6456 ULX and present results of the optical spectroscopy.

2. Astrometry

To identify the optical counterpart of UGC 6456 ULX, we used archival images from the Chandra X-Ray Observatory and HST. Chandra observed the source only once, on 2000 January 7 (ObsID 871). The source was positioned on the S3 chip of the Advanced CCD Imaging Spectrometer (ACIS) with a very small offset from the optical axis (<0.′1). The ULX coordinates in the ACIS image obtained with the Wavdetect task of CIAO 4.11 is R.A.(J2000) = $11^h\,28^m\,03\overset{s}{.}000$, decl. (J2000) = $+78°\,59'\,53\overset{''}{.}41$ with a statistic error of ∼0.″1 and an absolute astrometric uncertainty of 0.″8 at 90% confidence level.[3]

In the optical range, we have chosen the HST observation taken on 1994 February 16 with the Wide Field and Planetary Camera 2 (WFPC2) in the F555W filter. To apply astrometric corrections to the HST image, we used four reference stars that present in the Gaia Data Release 2 (Gaia Collaboration et al. 2018). After accounting for the shifts, derived standard deviation of the difference between Gaia and corrected HST positions of the reference stars became less than 0.″03, and the resultant absolute astrometric uncertainty about 0.″02 at the 90% confidence level.

There is only one relatively bright object in the WFPC2/F555W image within the Chandra 0.″8 error circle of UGC 6456 ULX (left panel of Figure 1). It is a point-like source with a visual magnitude of $m_{\rm F555W} = 21.59 \pm 0.06$ ($m_V = 21.58$) in the Vegamag system.[4] At the galaxy distance this corresponds to an absolute magnitude of $M_V = -6.9$ after correction for reddening of $A_V = 0.2$ mag (see Section 4).

3. X-Ray and Optical Variability

The ULX was observed 17 times with the X-ray telescope of the Neil Gehrels Swift Observatory (Swift/XRT) since 2011 January. From 2014 March 16 through 2014 April 6 the observations were made every few days. Exposure times were

[3] http://cxc.harvard.edu/cal/ASPECT/celmon/
[4] Photometry was performed on `c0f` image in HSTPHOT 1.1 (Dolphin 2000).

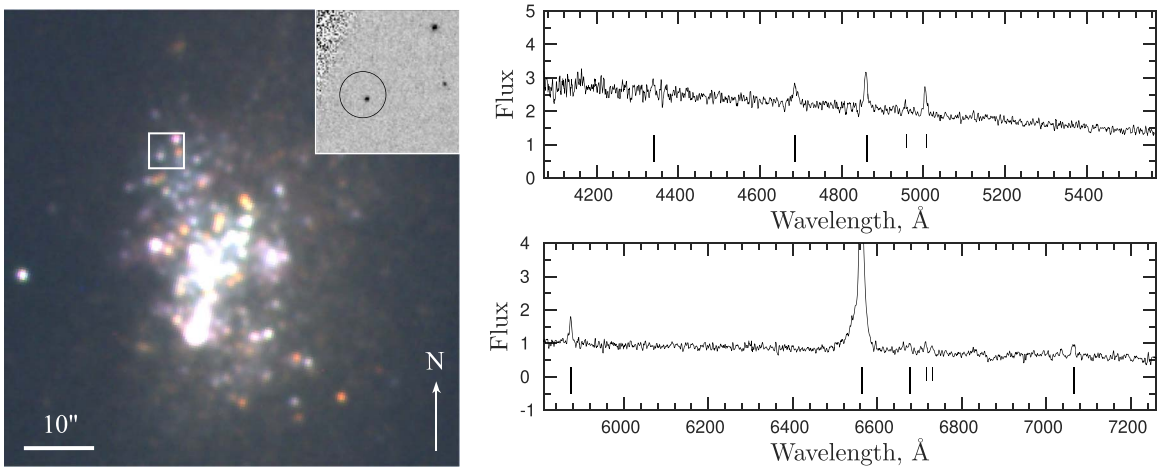

Figure 1. Left panel: superposition of B, V, and R_c images of the UGC 6456 galaxy taken with BTA/SCORPIO. The inset shows the HST/WFPC2/F555W image of the region around UGC 6456 ULX marked by the square; the circle indicate the $0\farcs8$ error box of the ULX position derived from the Chandra data. Right panel: blue (top) and red (bottom) spectra of the UGC 6456 ULX optical counterpart with the best signal-to-noise ratio. The spectra are not simultaneous. Broad emission lines are designated by long vertical bars; the narrow emissions produced by the nearest nebula are marked by short bars (see the text for details).

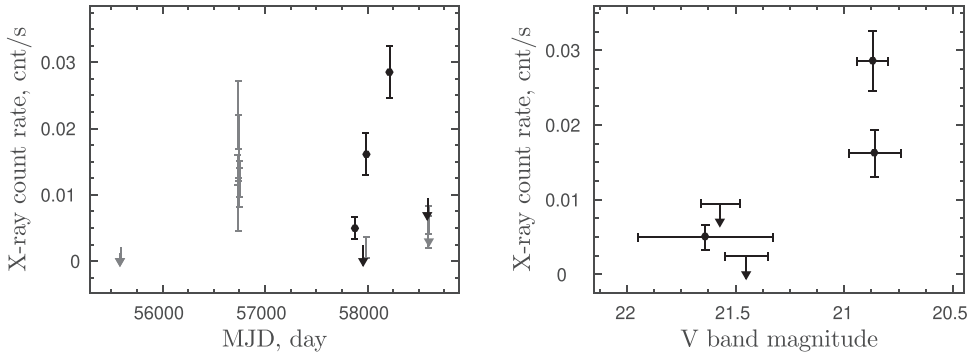

Figure 2. Left panel: net count of UGC 6456 ULX in the 0.3–10 keV range measured from the Swift data. The data points shown by black symbols indicate those Swift observations that were carried out quasi-simultaneously with the optical ones (Table 1). The arrows show an 90% upper limit to the count rate for the observations that have accumulated less than four counts. Right panel: net count rate plotted against V-band magnitude obtained from the quasi-simultaneous observations.

in the range of 230–4170 s. To extract a light curve we utilized preprocessed event files provided by the UK Swift data center.[5] The source events were extracted from a circular region of 30″ radius using the XSELECT task of HEASOFT 6.26.1. The background was taken from an annulus with inner and outer radii of 80″ and 130″, respectively, centered on the source. The resulting light curve is shown in Figure 2.

Starting from 2017 April, we carried out five quasi-simultaneous observations with Swift/XRT and optical telescopes of SAO RAS in the V-band (the Zeiss-1000 equipped with a charge-coupled device (CCD) photometer and the 6 m telescope BTA with the multi-mode focal reducer SCORPIO Afanasiev & Moiseev 2005). The time intervals between the X-ray and optical observations were within 1 day in the bright state of the ULX and in the range from 1.6 to ≃6 days in the faint state (Table 1). An aperture photometry of the UGC 6456 ULX counterpart was done with the APPHOT package in IRAF. To check the object for variability we used four stars with colors similar to those of the object as reference sources. The seeing was from $1\farcs0$ to $2\farcs1$ in all the observations. The obtained magnitudes were converted to the Vegamag system using three relatively bright isolated stars whose magnitudes were measured from the HST/WFPC2/F555W data.

[5] https://www.swift.ac.uk

Table 1
Results of the Quasi-simultaneous X-Ray/Optical Observations

Date	Telescope	T_{exp}, s	Count Rate or V Magnitude
2017 Apr 30	Zeiss-1000	900	21.64 ± 0.31
2017 May 2	Swift/XRT	2055	$(5.0 \pm 1.7) \times 10^{-3}$
2017 Jul 21[a]	BTA	330	21.43 ± 0.16
2017 Jul 24[b]	Swift/XRT	1770	$<2.4 \times 10^{-3}$
2017 Jul 27[a]	Zeiss-1000	2400	21.48 ± 0.11
2017 Aug 15	BTA	360	20.86 ± 0.12
2017 Aug 16	Swift/XRT	1690	$(1.6 \pm 0.3) \times 10^{-2}$
2018 Apr 11	Zeiss-1000	1800	20.87 ± 0.07
2018 Apr 11	Swift/XRT	1840	$(2.9 \pm 0.4) \times 10^{-2}$
2019 Apr 6	Zeiss-1000	1200	21.57 ± 0.09
2019 Apr 13[b]	Swift/XRT	230	$<9 \times 10^{-3}$

Notes. We provide the net 0.3–10.0 keV count rate for the X-ray observations and the V-band magnitudes for the optical ones.
[a] This pair of the optical observations was averaged.
[b] Only a 90% upper limit to the count rate is provided due to low statistics.

During these quasi-simultaneous observations the Swift count rate changed by a factor of at least six, and the visual magnitude by $\Delta m_V \approx 0.8$ mag (from $M_V \approx -6.8$ to

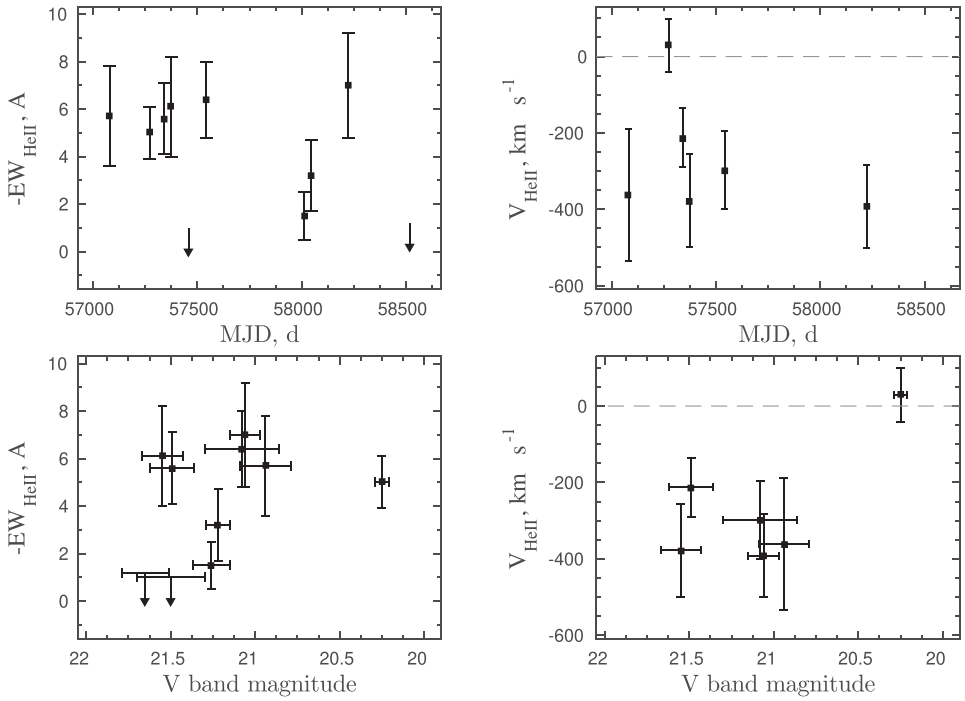

Figure 3. Top-left panel: variations of the equivalent width (EW) of the He II λ4686 emission line. The arrows indicate an 90% upper limit to the EW for those observations where the line was nearly undetectable. Two pairs of adjacent observations taken with a time interval of about one day with the VPHG1200G and VPHG550G grism were averaged. Top-right panel: radial velocity curve measured from the He II λ4686 emission line. Two data points near MJD = 58,000 are omitted due to a very low accuracy of the velocity measurements. Bottom-left panel: the EW of the He II line vs. the *V*-band magnitude. Bottom-right panel: the He II radial velocity vs. the *V*-band magnitude of UGC 6456 ULX.

$M_V \approx -7.6$). We found a correlation between the fluxes in these two bands (Figure 2, right panel) with a Pearson correlation coefficient of 0.9 ± 0.3, which corresponds to the *p*-vales of 0.07. Moreover, because the observations are not purely synchronous, the observed correlation might be underestimated because the X-ray flux demonstrate rapid changes (by a factor of three within one day).

4. Optical Spectroscopy

The optical spectra were obtained with the BTA/SCORPIO in 2015–2019; the 1″ slit and four grisms were used. In our work we use one observation conducted with the VPHG1200B grism (spectral range is 3600–5400 Å, resolution ≈5.5 Å), seven observations with VPHG1200G (4000–5700 Å, ≈5.3 Å), one with VPHG1200R (5700–7500 Å, ≈5.3 Å), and the remaining four observations with VPHG550G (3500–7200 Å, ≈12 Å). Seeing varied from 1″ to 2″. Data reduction was carried out with the LONG context in MIDAS using standard algorithm. The spectra were extracted with the SPEXTRA package (Sarkisyan et al. 2017).

Two spectra with the best signal-to-noise ratio are shown in the right panel of Figure 1. The spectra are not simultaneous. The first one taken with the VPHG1200R grism was obtained on 2015 February 23, whereas the second with VPHG1200G on 2015 September 7. A broad He II λ4686 line is clearly seen. Its width after correction for the spectral resolution is FWHM $= 880 \pm 80$ km s^{-1}. The blue spectrum also contains a weak broad component of the H_β emission line with the width comparable to that of the He II line, and also possibly contains H_γ emission and H_δ absorption lines. In the red spectrum, there are relatively broad He I emission lines with FWHMs (after correction for the spectral resolution) of 260 ± 80 km s^{-1} (He I λ5876) and 290 ± 50 km s^{-1} (He I λ7065). We also detected He I λ6678 line, but we can not reliable estimate its width due to low signal-to-noise ratio. A very strong and asymmetric H_α line has wings extending over 90 Å.

Narrow emission lines ([O III] $\lambda\lambda$4959,5007, [S II] $\lambda\lambda$6716,6731, as well as the narrow components of the H_β and H_α) can be formed in a nebula near the source (which, however, may be too compact and too weak to be seen in Figure 1).

All the wide lines are highly variable. We have investigated the behavior of the He II λ4686 line because it is not contaminated by the nebula emission. Its equivalent width (EW) varies from ≈ -7 to $\gtrsim -1$ Å (when the line is nearly undetectable; see the left panels of Figure 3) and the width from ≈500 to ≈900 km s^{-1}. We also found changes in the radial velocity up to 400 km s^{-1} (see the right panels of Figure 3), but additional observations are required to distinguish whether or not the nature of these changes is periodic or stochastic. Barycentric corrections are taken into account. We note that for the VPHG1200B and G observations the accuracy of the radial velocity measurements is better than 15 km s^{-1} and better than 30 km s^{-1} for the VPHG550G ones.

All the optical spectra were taken together with *V*-band images, which allows us to check a possible correlation between the He II EW and the optical brightness of the source. The photometry was performed by the same method as described in Section 3. We found that the object's *V* magnitude varied during these observations by $\Delta m_V = 1.40 \pm 0.15$ mag (from 21.65 ± 0.14 to 20.25 ± 0.04). The EWs and radial velocities of the He II λ4686 line versus the obtained *V* magnitudes are shown in bottom panel of Figure 3. It is seen that, in general, the |EW| is held near 5–6 Å regardless of the source optical brightness; however, when the source is faint the

line may sometimes weaken. The constancy of the line EW implies that the total flux in the line increases as the source become brighter. Analyzing simultaneous optical spectroscopy–X-ray observation of NGC300 ULX-1, Binder et al. (2018) found that the X-ray flux and the flux in the He II λ4686 are correlated. Our spectroscopic and X-ray observations are not simultaneous; nevertheless, combining the relation between the line flux and m_V with the relation between m_V and the X-ray count rate (Figure 2), we can conclude that similar correlation may occur in the case of UGC 6456 ULX as well. However, new observations are still needed to prove this to be more reliable. Another interesting feature is that the He II line showed the largest jump of the radial velocity when the source was in the brightest state.

Using observed ratios of the hydrogen lines in the nebula (H_γ/H_β and H_α/H_β), we determined the reddening value of $A_V = 0.2 \pm 0.1$ mag. In our calculation we assumed Case B of photoionization (Osterbrock & Ferland 2006). However, we have to note that it is unknown whether the nebula is associated with the ULX or it just lies on the line of sight. To clarify this, additional high-resolution observations in narrow filters are required. Nevertheless, all the nebulae in the area of the object show approximately the same reddening; therefore, we believe that the estimate of $A_V = 0.2 \pm 0.1$ mag is reliable regardless of the nature of the nebula whose lines are observed in the spectrum.

5. Conclusions

We have identified UGC 6456 ULX with the single optical source that falls into the astrometry error circle. The discovered optical counterpart is one of the brightest among all identified ULXs (M_V up to -8.24 ± 0.11; the A_V uncertainty was taking into account). The object demonstrates high optical and X-ray variability, and it has an amplitude that is similar to that observed in the well-studied ULX with neutron star NGC 7793 P13 (Fürst et al. 2018). We found a correlation between the optical and X-ray fluxes, which may indicate that the optical emission originates from re-processing of X-rays in the outer parts of the strong wind from the supercritical disk. The existence of such a wind is confirmed by the broad hydrogen and helium emission lines in the optical spectra that are typical for many spectroscopically studied ULXs (Fabrika et al. 2015).

Nevertheless, some ULXs show optical spectra that differ in varying degrees from each other and from the spectrum of UGC 6456 ULX. For example, M101 ULX-1 shows only broad helium and nitrogen emission lines belonging to a Wolf−Rayet donor (Liu et al. 2013), which indicates that this system is more evolved than UGC 6456 ULX, where the donor must be a hydrogen-rich star. The optical spectra of NGC 7793 P13 are dominated by emission from a B9Ia donor star (Motch et al. 2014): the spectra exhibit strong high-order Balmer absorption lines, as well as relative weak absorption lines of He I, Si II, Fe II, and Mg II. More typical for ULXs emission lines of hydrogen (up to H_γ), He II λ4686 and Bowen blend C III–N III are also present in the source spectrum; these lines may originate either from some structures of the accretion disk (like a disk bulge at the point where the stream of matter escaping L1 impacts the edge of the disk; Motch et al. 2011) or from the accretion disk wind. In contrast to this, the ultraluminous pulsar NGC 300 ULX-1 has a much more complex emission spectrum (Binder et al. 2018; Heida et al. 2019) indicating the presence of a $\approx$1000 km s^{-1} outflow and ionization by X-rays. In particular, the He II λ4686 line luminosity was found to be correlated with the soft X-ray emission. Our results hints that in the case of UGC 6456 ULX similar correlation also may be present.

We believe that the uniquely high optical brightness of UGC 6456 ULX and its isolation from other bright stars (together with high variability in both X-ray and optical bands) make this source the best target for studying the nature of optical emission from ULXs.

This study was funded by RFBR according to the research project 18-32-20214. This work made use of data supplied by the UK Swift Science Data Centre at the University of Leicester. We are grateful to A. Moskvitin and O. Spiridonova for their observations on Zeiss-1000. Observations with the SAO RAS telescopes are supported by the Ministry of Science and Higher Education of the Russian Federation (including agreement No05.619.21.0016, project ID RFMEFI61919 X0016).

ORCID iDs

A. Vinokurov https://orcid.org/0000-0001-5197-2457
K. Atapin https://orcid.org/0000-0002-8816-2017

References

Afanasiev, V. L., & Moiseev, A. V. 2005, AstL, 31, 194
Bachetti, M., Harrison, F. A., Walton, D. J., et al. 2014, Natur, 514, 202
Binder, B., Levesque, E. M., & Dorn-Wallenstein, T. 2018, ApJ, 863, 141
Brorby, M., Kaaret, P., & Feng, H. 2015, MNRAS, 448, 3374
Carpano, S., Haberl, F., Maitra, C., & Vasilopoulos, G. 2018, MNRAS, 476, L45
Colbert, E. J. M., & Mushotzky, R. F. 1999, ApJ, 519, 89
Dolphin, A. E. 2000, PASP, 112, 1397
Fabrika, S., Ueda, Y., Vinokurov, A., Sholukhova, O., & Shidatsu, M. 2015, NatPh, 11, 551
Fürst, F., Walton, D. J., Harrison, F. A., et al. 2016, ApJL, 831, L14
Fürst, F., Walton, D. J., Heida, M., et al. 2018, A&A, 616, A186
Gaia Collaboration, Brown, A. G. A., Vallenari, A., et al. 2018, A&A, 616, A1
Gladstone, J. C., Copperwheat, C., Heinke, C. O., et al. 2013, ApJS, 206, 14
Gladstone, J. C., Roberts, T. P., & Done, C. 2009, MNRAS, 397, 1836
Heida, M., Lau, R. M., Davies, B., et al. 2019, ApJL, 883, L34
Israel, G. L., Belfiore, A., Stella, L., et al. 2017, Sci, 355, 817
Liu, J.-F., Bregman, J. N., Bai, Y., et al. 2013, Natur, 503, 500
Motch, C., Pakull, M. W., Grisé, F., et al. 2011, AN, 332, 367
Motch, C., Pakull, M. W., Soria, R., et al. 2014, Natur, 514, 198
Osterbrock, D. E., & Ferland, G. J. 2006, Astrophysics of Gaseous Nebulae and Active Galactic Nuclei (Sausalito, CA: University Science Books)
Pinto, C., Middleton, M. J., & Fabian, A. C. 2016, Natur, 533, 64
Poutanen, J., Fabrika, S., Valeev, A. F., Sholukhova, O., & Greiner, J. 2013, MNRAS, 432, 506
Rodríguez Castillo, G. A., Israel, G. L., Belfiore, A., et al. 2019, arXiv:1906.04791
Sarkisyan, A. N., Vinokurov, A. S., Solovieva, Y. N., et al. 2017, AstBu, 72, 486
Sathyaprakash, R., Roberts, T. P., Walton, D. J., et al. 2019, MNRAS, 488, L35
Sutton, A. D., Roberts, T. P., & Middleton, M. J. 2013, MNRAS, 435, 1758
Tao, L., Feng, H., Grisé, F., & Kaaret, P. 2011, ApJ, 737, 81
Tully, R. B., Courtois, H. M., Dolphin, A. E., et al. 2013, AJ, 146, 86
Walton, D. J., Fürst, F., Heida, M., et al. 2018, ApJ, 856, 128